International Journal of Environmental Science and Technology (2022) 19:6429–6444
https://doi.org/10.1007/s13762-021-03576-9

ORIGINAL PAPER

Mechanistic evaluation of cationic dyes adsorption onto low-cost calcinated aerated autoclaved concrete wastes

M. Gheibi[1] · M. Eftekhari[2] · M. G. Tabrizi[3] · A. M. Fathollahi-Fard[4] · G. Tian[5,6,7]

Received: 21 January 2021 / Revised: 21 June 2021 / Accepted: 22 July 2021 / Published online: 9 August 2021

Abstract

Application of construction and demolition (C&D) wastes were considered as sustainable development goals (SDGs) for maintaining raw materials. Also, lightweight concretes such as aerated autoclaved concrete (AAC) were used for partitioning spaces in the building industry. Moreover, the waste products of the mentioned materials were increased due to the rise of old construction demolitions. This study contributes a calcinated aerated autoclaved concrete (CAAC) which is efficient, powerful, highly rapid, non-expensive and novel adsorbent for the removal of cationic dyes including malachite green (MG), methyl violet (MV) and methylene blue (MB) form water samples. The impacts of different variables for the proposed system including initial pH value, stirring rate, dye concentration and contact time are explored to optimize the selected analyses. Most notably, this study analyzes the experimental isotherm data by using two-parameter isotherms such as Dubinin–Radushkevich, Temkin, Langmuir and Freundlich equations and three-parameter isotherms including Koble–Corrigan, Toth, Redlich–Peterson and Sips models. The maximum adsorption capacities for MG, MB and MV are 370.4, 256.4 and 277.8 mg g^{-1}, respectively. In addition, five kinetic models, Elovich, intraparticle diffusion, main equations of pseudo-first- and second-order, and Boyd mathematical models are employed to follow the kinetic parameters and adsorption process of each dye. The Boyd equations indicate that with regard to all three dyes and at all concentrations, the film diffusion is dominant over intraparticle diffusions. Almost none of the geometric plots of adsorption and desorption curves intersected, indicating the adsorption process is optimally performed.

Keywords Calcinated aerated autoclave concrete · Methylene blue · Methyl violet · Malachite green · Adsorption kinetics and isotherm; Mathematical models

Introduction

The world has seen a great deal of interest in the global domestic industry sustainability grand challenge. The actual implementation of sustainability practices within the physical objects to environmental protection throughout the world is unsustainable economically, environmentally and socially (Tian et al., 2019; Liu et al., 2020; Yuan et al., 2020; Wang et al., 2020). The sustainable development issues are recent in today's economic activities, needing coordinated environmental protection systems, and enforce the decision-makers to focus on the environmental parameters based on

Editorial responsibility: Maryam Shabani.

✉ A. M. Fathollahi-Fard
amirmohammad.fathollahifard.1@ens.etsmtl.ca

[1] Department of Civil and Environmental Engineering, Ferdowsi University of Mashhad, Mashhad, Iran

[2] Department of Chemistry, Faculty of Sciences, University of Neyshabur, Neyshabur, Iran

[3] Department of Civil Engineering, Sharif University of Technology, Tehran, Iran

[4] Department of Electrical Engineering, École de Technologie Supérieure, University of Québec, Montréal, Canada

[5] School of Mechanical Engineering, Shandong University, Jinan 250061, China

[6] Key Laboratory of High Efficiency and Clean Mechanical Manufacture (Ministry of Education), Shandong University, Jinan 250061, China

[7] National Demonstration Center for Experimental Mechanical Engineering Education, Shandong University, Jinan 250061, China

triple lines of sustainability, i.e., economic, environmental and social aspects simultaneously (Fathollahi-Fard et al., 2020a).

Given the dynamic economies of the developing countries, their domestic industries are often on a path of significant growth. Meanwhile, in the definitions of sustainable development, the environmental dimensions of such progress must be considered as well as the economic growth (Reife & Freeman, 1996). Among all the environmental factors and impacts due to the development of industries, the quantity and quality of the produced wastewater by the dyeing and textile industries can be mentioned as a type of such malicious wastewaters (Verma, 2008; Fathollahi-Fard et al., 2020b). As a result of consuming almost ten thousand types of dyes throughout the production process, textile industries are constantly considered as severe environmental pollutants (Vankar, 2000). The presence of dye materials in wastewater leads to reduced water transparency and sewage. Also, these types of contaminants are toxic, carcinogen and produce chronic epidemiologic effects (Srivastava et al., 2004).

Malachite green (MG) is an organic compound considering as a food coloring additive. It also presumes as a dye for paper, silk, cotton, jute, wool, and leather (Yang et al., 2019; Yu et al., 2021). Most notably, hazardous compounds such as MG has a significant role in healthcare systems. Accordingly, this organic compound is employed as a medical disinfectant and anthelminthic. In an aquaculture aspect, it is also a fungicide and antiseptic (Hashimoto et al., 2011).

Concerning the domestic industries, methylene blue (MB) is a popular dye in printing and dyeing industries, the mentioned pollutant can generate many diseases for the consumers. They may accumulate in the heart organ or the respiratory and digestive systems (Gillman, 2011). Methyl violet (MV) dye is used as a pH indicator in the dyeing of straw, silk, paper, leather, cotton, bamboo, etc. (Fathollahi-Fard et al., 2021; Mojtahedi et al., 2021). Additionally, MV dye presents naturally the effluent of many industries like the pharmaceutical, printing, plastic cosmetic, textile and steel industries (Sabnis, 2010). Several different methods are used to remove dye compounds present in water and sewage samples such as ionic exchange (Suteu et al, 2014), adsorption (Yang et al., 2015; Robati et al., 2016; Khan & Khan, 2015; Fu et al. 2015), coagulation and flocculation (Moghaddam et al., 2015), biological decomposition processes (Saratale et al., 2011), nanofiltration (Nataraj et al., 2009; Mo et al., 2008) and other membrane methods (Al-Bastaki, 2004). Aerated concrete is one of the lightweight materials which consist of silica, sand, Portland cement type (II), lime, quartz and aluminum powder (Jerman et al., 2013). Industrial production of aerated autoclaved concrete (AAC) or commercially Heblex blocks was performed in five stages including dosing and mixing, molding, casting, demolding cutting and heating. During casting, chemical reactions generate hydrogen gas which creates pores in the concrete and reduces its density (Hamad, 2014). Since lightweight materials reduce the weight of the structures, these compounds have great significance in constructions; therefore, these are a very worthy choice to replace with traditional bricks in constructions. With the developing building industry, AAC economic blocks usages increase dramatically, especially in Iran. It is more vital and necessary to consider AAC wastes for reutilization due to the integrated solid waste management (ISWM) (McDougall et al., 2008). The quantitative analysis of AAC materials typically has exhibited, 45–50% SiO_2, 20–25% CaO, 1–5% Al_2O_3 and below 5% of Fe_2O_3, K_2O, Na_2O, MgO and TiO_2 (29). Regarding the aforementioned chemical compositions, the AAC compound has the same adsorptive behavior as the zeolite group (Hartmann & Buhl, 2012). Based on searches of scientific databases, the adsorbent applied in this study is novel and so far no research has been done on this subject. Tang et al. have achieved maximally capacity of adsorption as 129 mg g^{-1} for MB dye using H_3PO_4 modified corn stalks (P-CSs) (Tang et al., 2019). Porkodi and Kumar have presented a capacity of adsorption maximally as 136.6 mg g^{-1} for MG dye applying jute fiber carbon as an adsorbent (Porkodi and Kumar, 2007). Moreover, with the use of nanoclay modified by hydrogels of polyacrylic acid, Bhattacharyya and Kumar Ray have reached 111 mg g^{-1} maximum adsorption capacity for MV dye (Bhattacharyya & Ray, 2015); and according to the obtained results, calcinated aerated autoclaved concrete (CAAC) waste is an appropriate candidate to use as a significant adsorbent for the removing of cationic dyes from water samples (Sasmal et al., 2020; Tang et al., 2020). It goes without saying that according to the evaluation of researches, the application of local construction and demolition (C&D) wastes with focusing on sustainability were utilized less than other adsorbents (Kumar et al., 2016; Hor et al., 2016; Kuppusamy et al., 2016).

The key point of contribution in this paper is novel CAAC wastes as an efficient adsorbent for highly rapid removal of the cationic dyes such as MV, MG and MB from water samples. The critical factors which have a high impact on the removal efficiency including pH, amounts of adsorbent, stirring rate and contact time are analyzed and addressed. Equilibrium study of the present research was evaluated by two-parameter (Dubinin–Radushkevich, Temkin, Langmuir, and Freundlich) and three-parameter (Koble-Corrigan, Toth, Redlich–Peterson, and Sips) isotherms. As such, five kinetic models, the equations of pseudo-first- and second-order, Elovich, intra-particle diffusion, and Boyd equations, are studied to follow the adsorption process. Most notably, for

each dye, kinetic parameters are calculated and discussed. Based on the recent advances in this research area and information obtained from scientific databases, no study has treated the CAAC wastes as an adsorbent for decontamination of dyes; and according to the obtained results, CAAC waste is a worthy candidate to use as an effective powder for eliminating cationic dyes from water samples.

Materials and methods

Material

In current analyses, deionized water was used for preparing each solution. MG, MB and MV cationic dyes were provided from Sigma-Aldrich, USA, with 364.91, 333.6 and 393.96 g mol^{-1} molecular weight, respectively. Additionally, the mentioned dyes were detected in λ_{max} equal to 620 nm (MG), 660 nm (MB), and 580 nm (MV). The structures of MG, MB and MV are depicted in Fig. S1. The CAAC block wastes (Fig. S2) were prepared from the Razavi HEBELEX factory in Mashhad, Iran.

The manufacturer was asked to specifically use 20% more lime to produce these samples, so the term calcinated was used in naming the final product. Finally, the sample used in the experiments named CAAC. The CAAC wastes were ground and sieved by 100 µm mesh. The obtained powder was treated before being utilized in the present experiments. The suspension containing 15 g L^{-1} CAAC powder mechanically was stirred for 1 h, and then the mentioned powder was filtered using filter paper; this protocol was done for another time. Finally, the solid sample was dehydrated completely during 24 h at 60˚C and applied in further experiments.

Instruments

This study has employed the UV–Vis spectrophotometer, Agilent 8453 including a photodiode-based detector with a glass cell considering 1 cm longitudinal path to obtain the spectrum in the range of 375–900 nm wavelengths. It should be noted that in the aqueous phase, pH values are adjusted via a pH meter containing glass-electrode (Metrohm 827 pH lab, Switzerland). Concerning the phase of separating, a Scientific Centurion Centrifuge (Model Andreas Hettich D72, Tuttlingen, Germany) was engaged. An AVATAR 370 (USA) FT-IR spectrometer was applied to record the Fourier Transform Infrared (FTIR) spectrum. Besides, a PW 1480 device (Netherlands, Philips Company) was utilized to carry out the X-Ray Fluorescence (XRF). Moreover, the morphology of CAAC adsorbent was evaluated by scanning electron microscope (SEM) model Philips S360 (Oxford, England, UK). N_2 adsorption–desorption isotherms belonged to the BET specific surface area was performed by Belsorp mini II, Japan.

Removal procedure

50 mL of MG, MV, and MB solutions containing 50 mg L^{-1} concentration was adjusted at pH 8.5, and then 0.1 g of CAAC powder was added to them. The resulting solutions were mixed for 25 min by magnetic stirrer at 400 rpm. By centrifuging the solutions at 2000 rpm for 2 min, the concentration of each dye was calculated according to its calibration curve.

The residual dye concentration in the adsorbent stage was computed by Eq. 1:

$$q_e = \frac{(C_0 - C_e)V}{m} \quad (1)$$

In the above equation, q_e is the adsorption capacity (mg g^{-1}) and C_e and C_0 are the equilibrium and initial concentrations of dyes in mg L^{-1}. In addition, V is known as a sample volume in litter. Likewise, m is the amount of CAAC powder in gram.

Adsorption isotherm models

Most importantly, isotherm models establish the most suitable linear and nonlinear regression coefficient for the equilibrium curves. To this end, different isotherm equations including two-parameter isotherms such as Freundlich, Langmuir, Dubinin–Radushkevich, and Temkin equations in addition to three-parameter isotherms like Sips, Redlich–Peterson, Toth, and Koble–Corrigan are employed.

Adsorption kinetic and geometric models

The purpose of the kinetic assessment for the process of adsorption is to examine its mechanism and limiting steps. The kinetic of cationic dyes adsorption was apprised by the pseudo-first and second-order, Elovich, intraparticle diffusion and Boyd mathematical formula (Mohan & Singh, 2002). The Geometric model aims to study the mechanism of adsorption and desorption and their change rates over time. In this study, based on the requirement of analyzing isotherm and kinetic mechanism, adsorption and desorption models have been developed based on the Langmuir (for Langmuir-based isotherms) and Langmuir–Freundlich models (For Freundlich based isotherms) (Azizian et al., 2007).

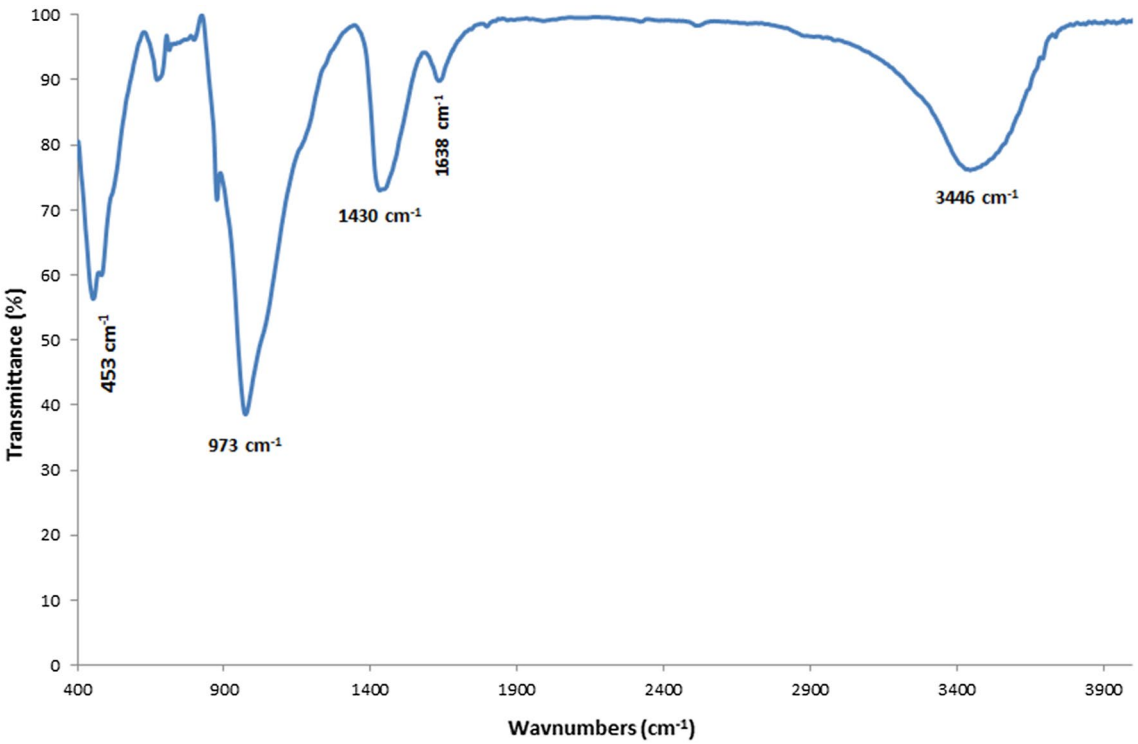

Fig. 1 FT-IR spectrum of CAAC powder

Results and discussion

Characterization of CAAC powder

To determine the composition of CAAC powder, XRF is analyzed on the adsorbent and the results are presented in Table S1. The XRF measurement shows that the main chemical compositions of CAAC powder are SiO_2 (52.4%), CaO (37.3%), Al_2O_3 (3.6%), Fe_2O_3 (1.48%) and MgO (1.6%), K_2O (0.6%) and Na_2O (0.1%). The FT-IR spectrum of CAAC powder is revealed in Fig. 1. As it shows, the bending modes and Si–O-Si stretching of the calcium-silicate hydrate phases located at 900–1100 cm^{-1} and 675 cm^{-1}, respectively; plus, interior SiO_4 deformation mode was observed at 445 cm^{-1} (Hartmann & Buhl, 2012; Yu et al., 1999). Finally, the broad peak at 3440 cm^{-1} is related to the vibration of OH groups (Si–O-H) on the surface of CAAC adsorbent and the peak at 1634 cm^{-1} represents H–O-H bending vibration of water (Zaitan et al., 2008). Moreover, the SEM image with 20 and 10 µm resolutions is illustrated in Fig. S3. According to the results, it contains a number of irregular sheet particles mostly composed of CSH-phases (calcium silicate hydrate).

The BET analysis was employed to determine the surface area of the CAAC adsorbent. The surface area of the adsorbent plays a key role in adsorption phenomena so that by increasing of the surface area the available active sites for interaction by analyte increase effectively. The BET and BJH spectrum of CAAC adsorbent is presented in Fig. 2. According to IUPAC classification, it exhibits typical Type IV isotherm with an obvious hysteresis loop at P/P0 = 0.55–0.98) which corresponds to the presence of large amount of mesopores–micropores. Also, the hysteresis exists due to the presence of slit shaped pores (H3). According to the results, the obtained surface area and total pore volume were 24.64 $m^2\ g^{-1}$ and 0.4681 $cm^3 g^{-1}$, respectively. Also, the average pore diameter was 37.3 nm and in the range of mesopores adsorbents (2–50 nm).

pH Evaluation and adsorption mechanism

The pH of sample solutions influences the surface charge of the adsorbents in addition to the level of different contaminations ionization. The sorption of MB, MV and MG is investigated in the pH ranges of 3–10. Figure 3 reveals the impact of pH on the adsorption capacities of MG, MB and MV on CAAC powder. As the results have shown, the adsorption capacities of dyes were increased by increasing pH value

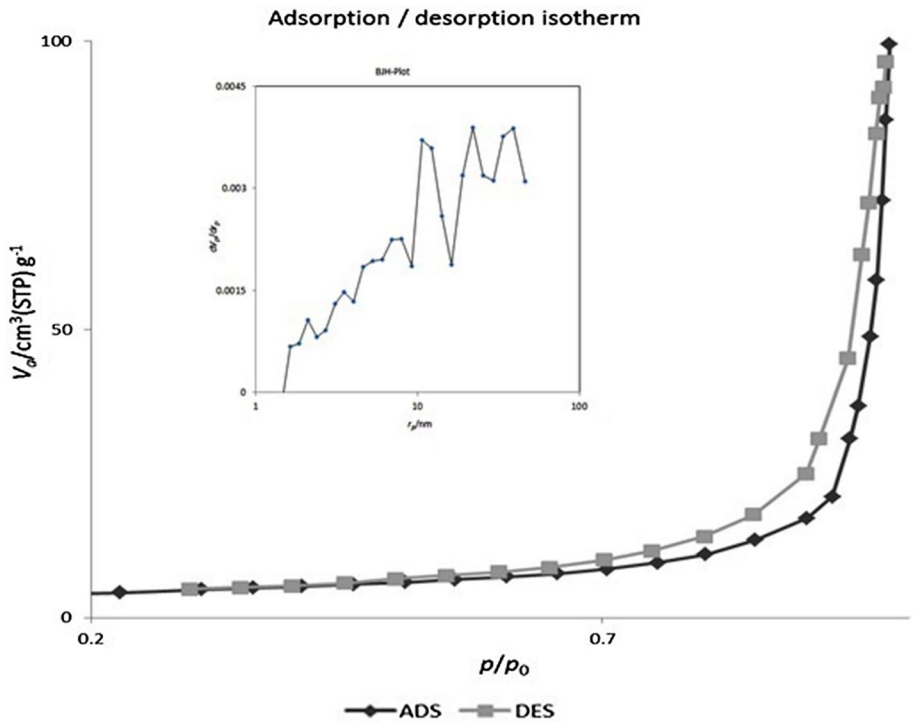

Fig. 2 Nitrogen adsorption–desorption isotherm and BJH pore width distribution (inset) of CAAC

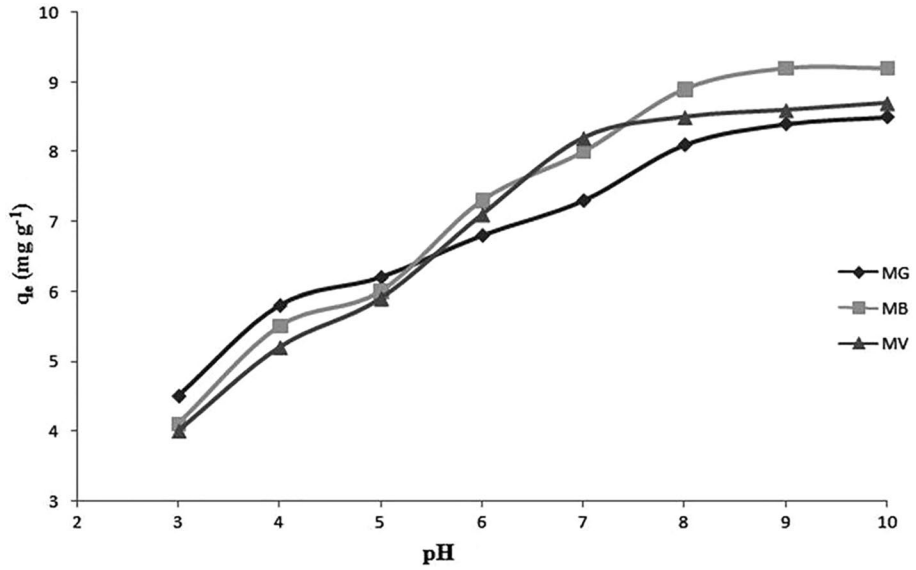

Fig. 3 Sample solution pH versus adsorption capacities (q_e) for MG, MB and MV dyes. Dyes concentrations: 50 mg L^{-1}, contact time: 60 min, temperature: 25 °C, CAAC powder: 0.1 g 50 mL^{-1}

which could be related to the negative charge of the adsorbent at basic pH values. The pH_{PZC} value for CAAC powder was 3.4; at pH values below than PZC (point of zero charge), the CAAC had a net positive charge and electrostatically repel cationic dyes. However, by increasing pH values, the positive charges on the cationic dyes are attracted by anionic sites of adsorbent (Weng & Pan, 2007). In CAAC-aqueous solution systems, the potential of the surface is determined by the activity of H^+ ions (or pH), which react with the CAAC surface. At $pH > pH_{Pzc,}$ the broken Si–O^- bonds on the surface of CAAC increases; therefore, it could be expect that at high pH values (pH = 8–10), the adsorption capacity increases due to the increasing of the available active sites. In conclusion, pH 8.5 was designated as the optimum value for the adsorption of all dyes investigated in this study.

Stirring rate evaluation

To examine the impact of stirring rate against the adsorption capacities of contaminations, it was investigated at

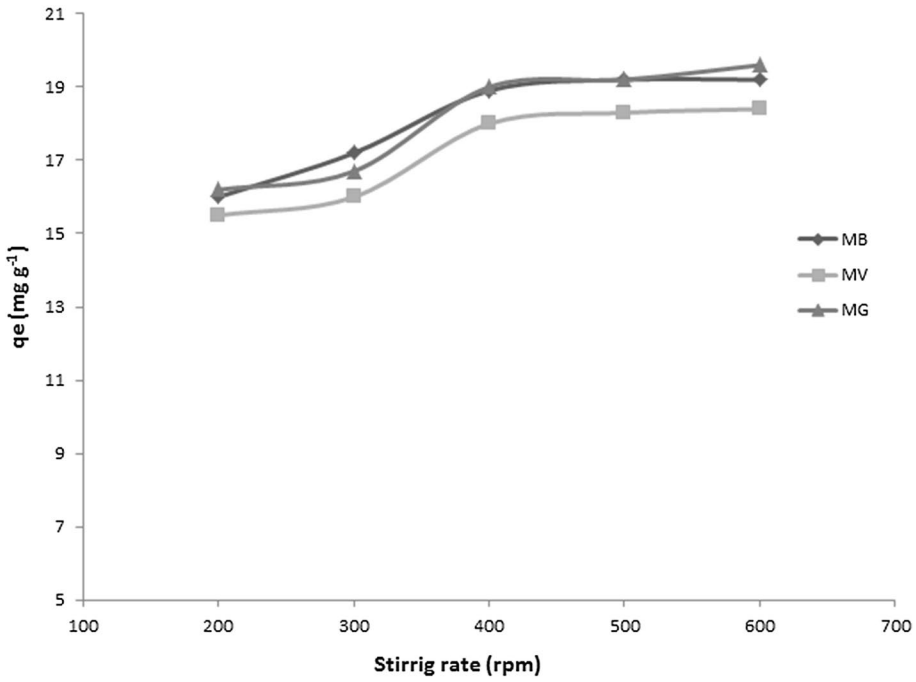

Fig. 4 Stirring rates versus adsorption capacities (q_e) for MG, MB and MV dyes. Dyes concentrations: 100 mg L^{-1}, contact time: 60 min, temperature: 25 °C, CAAC powder: 0.1 g 50 mL^{-1}

200—600 rpm for 50 mg L^{-1} initial dye concentrations and 25 °C temperatures. Regarding the obtained results in Fig. 4, stirring rate higher than 400 rpm has no significant impact on the adsorption of dyes. Therefore, 400 rpm stirring speed was taken for all dyes in further experiments.

Initial concentration and contact time evaluation

The impact of contact time and initial dyes concentrations on the adsorption capacities of MG, MB and MV is presented in Fig. 5 parts a, b, and c. As can be seen, the adsorption capacities of all dyes raised with an increase in the contact time up to 20 min. Also, increasing of dyes concentrations accelerate the mass transfer of MG, MB, and MV from the bulk solution onto the CAAC powder to diffuse into the mesopore structure of CAAC. Therefore, 25 min removal time was considered as the optimum contact time for the removal of all dyes.

Equilibrium study

Two-parameter isotherm models

Langmuir isotherm Regarding the monolayer adsorption, by plotting of C_e/q_e vs. C_e, the linear mathematics is employed for the Langmuir isotherm model (Eq. 2). The computations of K_{ads} (constant of Langmuir isotherm, mg L^{-1}) and Q_{max} (theoretical maximum capacity of adsorption, mg g^{-1}) are calculated from the intercept and slope of the plot, respectively, and the outcomes are presented in Table 1.

$$\frac{C_e}{q_e} = \frac{C_e}{Q_{\max}} + \frac{K_{ads}}{Q_{\max}} \tag{2}$$

Also, the practical maximum adsorption capacities of the studied dyes onto the CAAC powder have been determined by plotting of q_e vs. C_e for each dye, which are equal to 177.5, 125 and 128 mg g^{-1} for MG, MB and MV, correspondingly. As the correlation coefficients (R^2) of MG, MB and MV for the Langmuir isotherms are 0.98, 0.99 and 0.98, respectively; this proposes that the Langmuir mathematical model offers an upright model of the adsorption process ($R^2 > 0.90$).

Freundlich isotherm Moreover, the Freundlich mathematical model utilized for the multilayer heterogeneous surface sorption is revealed by Eq. 3.

$$\log q_e = \log K_F + \frac{1}{n} \log C_e \tag{3}$$

n and K_F are known as the favorability and adsorption capacity (mg g^{-1}) (Santhi et al., 2010), sequentially. By sketching of log q_e versus log C_e for each contaminant; these outcomes were computed and are displayed in Table 1. The correlation coefficients (R^2) of MG, MB and MV for the Freundlich isotherm model are 0.99, 0.99 and 0.98, correspondingly; which show that the Freundlich isotherm is analogous to the Langmuir equation for the studied dyes. Also, the values of $n > 1$ depict a desirable adsorption (Nekouei et al., 2015); and according to the n results of the studied dyes, all dyes are favorable for CAAC powder.

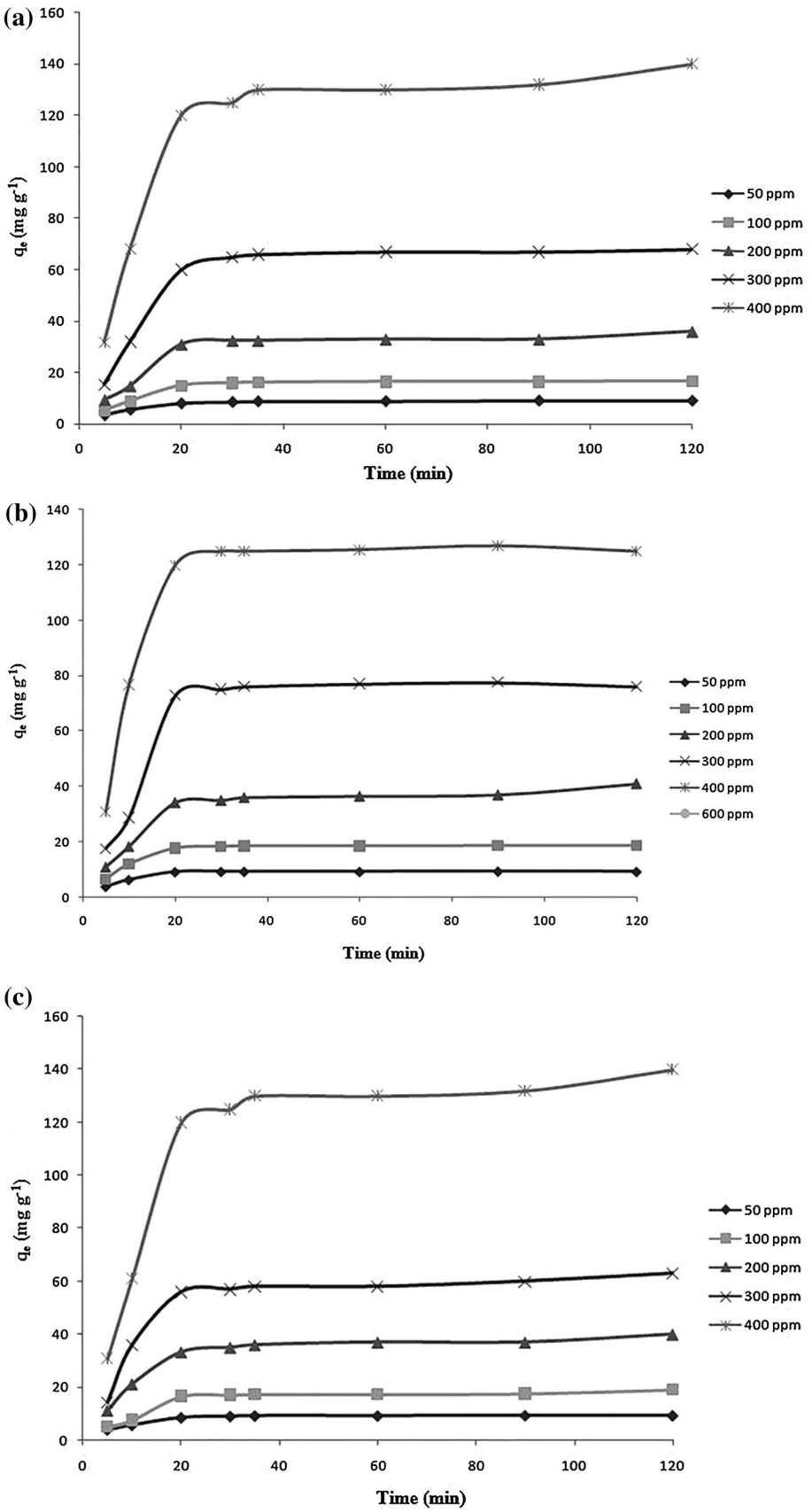

Fig. 5 Adsorption capacities of dyes vs. contact time for **a** MG **b** MB and **c** MV on CAAC powder at different dyes concentration. Conditions: pH 8.5, CAAC powder: 0.1 g in 50 mL

Table 1 Two-parameter isotherm factors for MG, MB and MV adsorption onto the CAAC

Two-parameter isotherm name	Parameter	MG	MB	MV
Langmuir	Q_m (mg g^{-1})	370.4	256.4	277.8
	K_a	354.4	129	174
	R^2	0.98	0.99	0.98
Freundlich	1/n	0.798	0.631	0.697
	K_f	1.74	4.59	3.14
	R^2	0.99	0.99	0.98
Temkin	α (L g^{-1})	0.086	0.196	0.137
	ß (mg L^{-1})	53.11	42.45	46.44
	b	46.67	58.39	53.38
	R^2	0.96	0.94	0.95
D-R	Q_m (mg g^{-1})	105.7	99.44	104.05
	K ($\times 10^{-5}$)	3	0.5	1
	E (J mol^{-1})	129.1	316.22	223.61
	R^2	0.63	0.55	0.6

Temkin isotherm Declining particles energy in adsorption reactions within the film layer is interpreted from the Temkin mathematical model. Due to the adsorbent–contamination synergies, the mentioned energy is decreased linearly. Plus, the adsorptive reaction is designated by a uniform distribution approximated by the binding energies (Santhi et al., 2010). The Temkin mathematical model is provided by Eq. 4:

$$q_e = \frac{RT}{b} \ln(K_T C_e) \tag{4}$$

Temkin linear form is shown as Eq. 5:

$$q_e = \beta \ln \alpha + \beta \ln C_e \tag{5}$$

It should be noted that, as $\beta = RT/b$. T, R and α are known as temperature (Kelvin), the universal gas constant (8.314 J K^{-1} mol^{-1}), and K_T, respectively. The fixed parameter of b is related to the adsorption heat (Santhi et al., 2010). Table 1 depicts all regression analysis factors and constants of the Temkin mathematical model (α, ß, b and R^2) for each contaminant. The amounts of R^2 for the MG, MB and MV are 0.96, 0.94 and 0.95, sequentially, which show that the Temkin isotherm is comparable to the Langmuir and Freundlich isotherms. However, the b constant value less than 8 kJ mol^{-1} shows that the surface adsorption occurs physically (Santhi et al., 2010). According to Table 1, b parameter values for MG, MB and MV dyes were found to be 0.467, 0.584 and 0.534 kJ mol^{-1}, correspondingly. Therefore, Temkin isotherm proposes physical interaction as the main process among contaminants and adsorbent.

Dubinin-Radushkevich (D-R) isotherm The D–R equation is shown through Eqs. 6 and 7:

$$q_e = Q_m \exp(-K\varepsilon^2) \tag{6}$$

$$\ln q_e = \ln Q_m - K\varepsilon^2 \tag{7}$$

where Q_m, K and ε convey the theoretical capacity of adsorption (mg g^{-1}), D–R constant (linked to the energy of adsorption), and Polanyi potential (ε) determined from Eq. 8 (Bulut et al., 2008).

$$\varepsilon = RT\, ln(1 + 1/C_e) \tag{8}$$

The slope of ln q_e versus ε^2 plot provides K and with the aid of the plot intercept value, the amounts of Q_m could be determined. It was determined from the K parameter according to Eq. 9 (Bulut et al., 2008):

$$E = \frac{1}{\sqrt{2K}} \tag{9}$$

The computed amounts of D-R parameters for MG, MB, and MV are given in Table 1. The contents of E were found in the range of 0.129–0.316 kJ/mol. As $E < 8$ kJ mol^{-1}, it proposes that the adsorption mechanism happens physically (Bouabidi et al., 2018) and the obtained results verify the Temkin isotherm. Also, the low R^2 values of the studied dyes (0.63, 0.55 and 0.6 for MG, MB and MV, respectively) show that Dubinin-Radushkevich isotherm is inapplicable for interpretation of experimental data.

Three-parameter isotherm models

Sips isotherm Sips isotherm is suitable to predict the adsorption process on the heterogeneous surface (Sips, 1948; Pérez-Marín et al., 2007). This model is expressed as Eq. 10:

$$q_e = \frac{K_S C_e^{\approx s}}{1 + a_S C_e^{\approx s}} \tag{10}$$

where K_S, C_e and β_S are Sips equilibrium constant (L mg^{-1}), the equilibrium concentration of contaminant (mg L^{-1}) and Sips isotherm equation exponent, respectively. If β_S convergence to one or equals to one, the model tends to the Langmuir model.

The values of Sips isotherm parameters for MG, MV and MB are reported in Table 2. As such, the values of R^2 were found to be in the range of 0.993–0.999 which shows the high applicability of the results to this model. According to Table 2, the parameter β_S for MG and MB tend to unity; therefore, these results suggest that the adsorption

Table 2 Three-parameter isotherm factors for MG, MB and MV adsorption onto the CAAC

Dye	Isotherm model	Parameter		R^2	Prescription
MG	Redlich–Peterson	K_R	1.173	0.997	Verifying Langmuir Isotherm model
		a_R	0.003		
		G	1.022		
	Koble–Corrigan	A	0.839	0.997	Verifying Langmuir Isotherm model
		B	0.003		
		N	1.084		
	Sips	K_s	0.839	0.997	Verifying Langmuir Isotherm model
		a_s	0.002		
		β_s	1.084		
	Toth	a_T	255.167	0.997	Verifying Langmuir Isotherm model
		K_T	241.076		
		T	1.046538		
MB	Redlich–Peterson	K_R	1.796	0.996	Verifying Langmuir Isotherm model
		a_R	0.009		
		G	0.942		
	Koble–Corrigan	A	2.165	0.998	Verifying Langmuir Isotherm model
		B	0.007		
		N	0.933		
	Sips	K_s	2.165	0.999	Verifying Langmuir Isotherm model
		a_s	0.007		
		β_s	0.933		
	Toth	a_T	132.15	0.999	Verifying Langmuir Isotherm model
		K_T	153.203		
		T	1.091		
MV	Redlich–Peterson	K_R	1.0466	0.997	Verifying Freundlich isotherm model
		a_R	0.005		
		G	1.616		
	Koble–Corrigan	A	0.630548	0.993	Verifying Freundlich isotherm model
		B	0.002		
		N	1.224		
	Sips	K_s	0.631	0.993	Verifying Freundlich isotherm model
		a_s	0.002		
		β_s	1.224		
	Toth	a_T	397.682	0.995	Verifying Freundlich isotherm model
		K_T	1321.868		
		T	0.655		

of the mentioned dyes followed the Langmuir isotherm; however, the value of β_S for MV is equal to 1.224, so its adsorption followed the Freundlich isotherm.

Redlich–Peterson (R–P) isotherm R–P is a type of hybrid model consisting of both Freundlich and Langmuir isotherms that combines three-parameters in the empirical equation (Redlich and Peterson, 1959). Due to its high versatility, it can be implemented to both heterogeneous and homogeneous systems. The proposed isotherm is expressed in Eq. 11:

$$q_e = \frac{K_R C_e}{1 + (a_R C_e)^g} \tag{11}$$

where g is the R–P equation exponent and the a_R (L mg^{-1}), K_R (L g^{-1}) are R-P constants. If g is equal to one or convergence to one, this model tends to the Langmuir model (Jossens et al., 1978). The values of the R–P isotherm model

for MG, MV and MB are listed in Table 2. The R^2 values considering MG, MB, and MV are 0.997, 0.996 and 0.997, correspondingly, which show that the R-P isotherm has preferable versatility to this research. According to Table 2, the amounts of g parameters were found to be 1.022, 0.942 and 1.616 for MG, MB, and MV, respectively. Based on the results, the adsorption of MG and MB followed the Langmuir isotherm; however, the adsorption of MV followed the Freundlich model.

Toth isotherm model In comparison with the Sips equation, the Toth isotherm is an aggregate of the Freundlich and Langmuir isotherm (Toth, 1971). In general, this isotherm assumes the quasi-Gaussian distribution at site affinity. Due to that fact, this isotherm applies to both relatively high and low pressures for Henry's law type behavior (Vijayaraghavan et al., 2006). Toth isotherm is expressed in Eq. 12.

$$q_e = \frac{K_T C_e}{(a_T C_e)^{\frac{1}{t}}} \tag{12}$$

where K_T and a_T are both Toth constants (mg g^{-1} and L g^{-1}, respectively). The parameter t is a Toth isotherm constant which represents heterogeneity factor. If t value is equal to one or convergence to one, the model is likely to the Langmuir mathematical model. The values of the Toth isotherm model for MG, MV and MB are given in Table 2. According to the results, the R^2 values placed in the range of 0.995–0.999, which shows the high adaptability of Toth isotherm. Due to the values of the t parameter obtained from Table 2, the Toth isotherm model proposes that the Freundlich equation well predicted for adsorption of MV dye. On the other hand, the Langmuir isotherm model is a convenient predictive model for MG and MB adsorption behavior.

Koble–Corrigan Isotherm (K–C isotherm) As mentioned earlier, another three-parameter practical model related to a mixture of Freundlich and Langmuir isotherms is the Koble–Corrigan isotherm equation (Koble & Corrigan, 1952). The nonlinear form of Koble–Corrigan isotherm is displayed in Eq. 13:

$$q_e = \frac{\mathrm{A}C_e^N}{1 + \mathrm{B}C_e^N} \tag{13}$$

where B and A are Koble–Corrigan constants (L^N mg^{1-N} g^{-1} and L^N mg^N) and N is the adsorption intensity. If the N values are equal to one or lean toward one, this model proposes that the Langmuir isotherm is more applicable than the Freundlich isotherm. The values of the K–C isotherm model are exposed in Table 2. According to the R^2 values ($R^2 > 0.99$), the high versatility of the K–C isotherm was observed for interpreting of the adsorption of all dyes onto the CAAC adsorbent. Also, based on the N values represented in Table 2, the adsorption of MG and MB followed the Langmuir isotherm; however, because of N value, K-C isotherm suggests the Freundlich isotherm as a well-described equation for the adsorption of MV.

Kinetic study

Pseudo-first-order kinetic

The kinetic adsorption values were represented via the pseudo-first-order, as known as the primary mathematical calculation considering the adsorption capacity. The differential mathematical model commonly manifests as Eqs. 14 and 15:

$$\frac{dq_t}{q_t} = k_1(q_e - q_t) \tag{14}$$

$$\log\left(\frac{q_e}{q_e - q_t}\right) = \frac{k_1}{2.303}t \tag{15}$$

The linear form of the pseudo-first-order kinetic model is expressed in Eq. 16:

$$\log(q_e - q_t) = \log q_e - \frac{k_1}{2.303}t \tag{16}$$

By drawing of log $(q_e - q_t)$ versus t for each dye (Figs. S4-S6), k_1 and q_e could be discovered from the slope and intercept of the plot, sequentially. The values of k_1, q_e, and R^2 for MG, MB, and MV are presented in Table S2. As can be seen, the R^2 values ($R^2 \geq 0.98$ for all dyes) designated that the examined dyes adsorption supported by the pseudo-first-order kinetic model. Furthermore, during the pseudo-first-order, calculated q_e values for the mentioned dyes are quite near to the experimental q_e amounts (Table S2) which explicitly confirm that the sorption kinetics of the investigated dyes are characterized by the pseudo-first-order kinetic model.

Pseudo-second-order kinetic

Kinetically evaluation of adsorption could be interpreting by considering pseudo-second-order equation according to Eq. 17 (Hamad, 2014).

$$\frac{dq_t}{q_t} = k_2(q_e - q_t)^2 \tag{17}$$

The k_2 parameter is known as the present model constant rate (g min^{-1} mg^{-1}). By regarding that $q_t = 0$ (at $t = 0$), the subsequent Eq. (18) is achieved:

$$\frac{t}{q_t} = \frac{1}{k_2 q_e^2} + \frac{1}{q_e}t \tag{18}$$

where the primary rate of sorption known as h (mg min^{-1} g^{-1}), at $t \to 0$ is described by: $h = q_e{}^2 k_2$.

Figs. S7-S9 show the t/q_t versus t plot for MG, MB and MV, where the values of q_e and h are gained from the slope and intercept, respectively. The results of h, R^2 and k_2 are presented in Table S3. According to the outputs, the amounts of R^2 for MB and MV are comparable to the pseudo-first-order kinetic. However, for MG dye, the R^2 values are moderate and placed in the range of 0.91–0.96. As well, the computed q_e amounts for the studied dyes are far from the experimental q_e (Table S3). Consequently, the gap between the amounts of experimental and computational q_e values indicate the inapplicability of the pseudo-second-order kinetic model to predict some adsorption factors.

Elovich model

Kinetically appraisal of Elovich model is expressed according to the adsorption behavior, which is usually represented as Eq. 19 (Hamad, 2014):

$$\frac{dq_t}{q_t} = B_E \exp(-A_E q_t) \tag{19}$$

where B_E and A_E are the primary rate of adsorption (mg g^{-1} min^{-1}) through experiments and the desorption constant (g mg^{-1}), respectively.

Equation 19 could be abridged by considering $A_E B_E t >> t$ and implementing the following boundary terms: (a) $q_t = 0$ at $t = 0$ (b) $q_t = q_t$ at $t = t$ (Eq. 20).

$$q_t = \frac{\ln A_E B_E}{A_E} + \frac{\ln t}{A_E} \tag{20}$$

If the adsorption of the aforementioned dyes onto the CAAC adsorbent obeys the Elovich equation, a plot of q_t versus $\ln(t)$ has an intercept of $\frac{\ln A_E B_E}{A_E}$ and a slope of $(1/A_E)$. The calculated A_E, B_E and R^2 values are presented in Table 3. Based on the results, the R^2 value was found to be 0.95–0.99 for MG and higher than 0.98 were obtained for MB and MV; therefore, these values indicate that the adsorptive reaction of the mentioned contaminants onto the CAAC powder supports by the Elovich model.

Intraparticle diffusion

The intraparticle diffusion is a kinetic model for studying the rate of dyes adsorption onto the CAAC powder (Hamad, 2014). Plus, the intraparticle diffusion model is usually displayed as Eq. 21:

$$q_t = K_{dif} t^{(0/5)} + C \tag{21}$$

The plots of q_t versus $t^{1/2}$ for the studied dyes were found to be linear where K_{dif} (mg g^{-1} $min^{-0.5}$) interpreted as a slope and C (mg g^{-1}), which presents data about the boundary layer thickness, is the intercept of the line for each dye. The obtained values of K_{dif} and C for each dye are expressed in Table 3. The values of R^2 for this model (higher than 0.97) indicated that the adsorption of all dyes onto the CAAC powder obeyed the intraparticle diffusion. Nevertheless, the mentioned curves have intercept (C values in the range of 2.1 – 55.3 mg g^{-1} in Table 3) showing that the intraparticle

Table 3 The parameters provided from Elovich and intraparticle diffusion models considering various primary dyes dosages

Dye (mg L^{-1})	Dosage	Elovich equation			Intraparticle diffusion model		
		A_E	B_E	R^2	K_{diff}	C	R^2
MG	50	0.28	1.27	0.97	2.13	2.1	0.99
	100	0.15	2.71	0.95	3.86	4.6	0.99
	200	0.07	5.58	0.99	8.37	9.2	0.99
	400	0.02	18.5	0.96	32.35	26	0.99
MB	50	0.28	1.91	0.99	2.07	3.3	0.99
	100	0.14	3.73	0.99	4	6.2	0.99
	200	0.07	5.97	0.98	8.6	10.5	0.99
	400	0.02	22.1	0.98	30.92	37.3	0.99
MV	50	0.26	1.7	0.99	2.19	3	0.97
	100	0.16	4.23	0.99	3.68	7.1	0.97
	200	0.07	6.84	0.99	8	11.3	0.99
	400	0.02	31.8	0.99	24.3	55.3	0.99

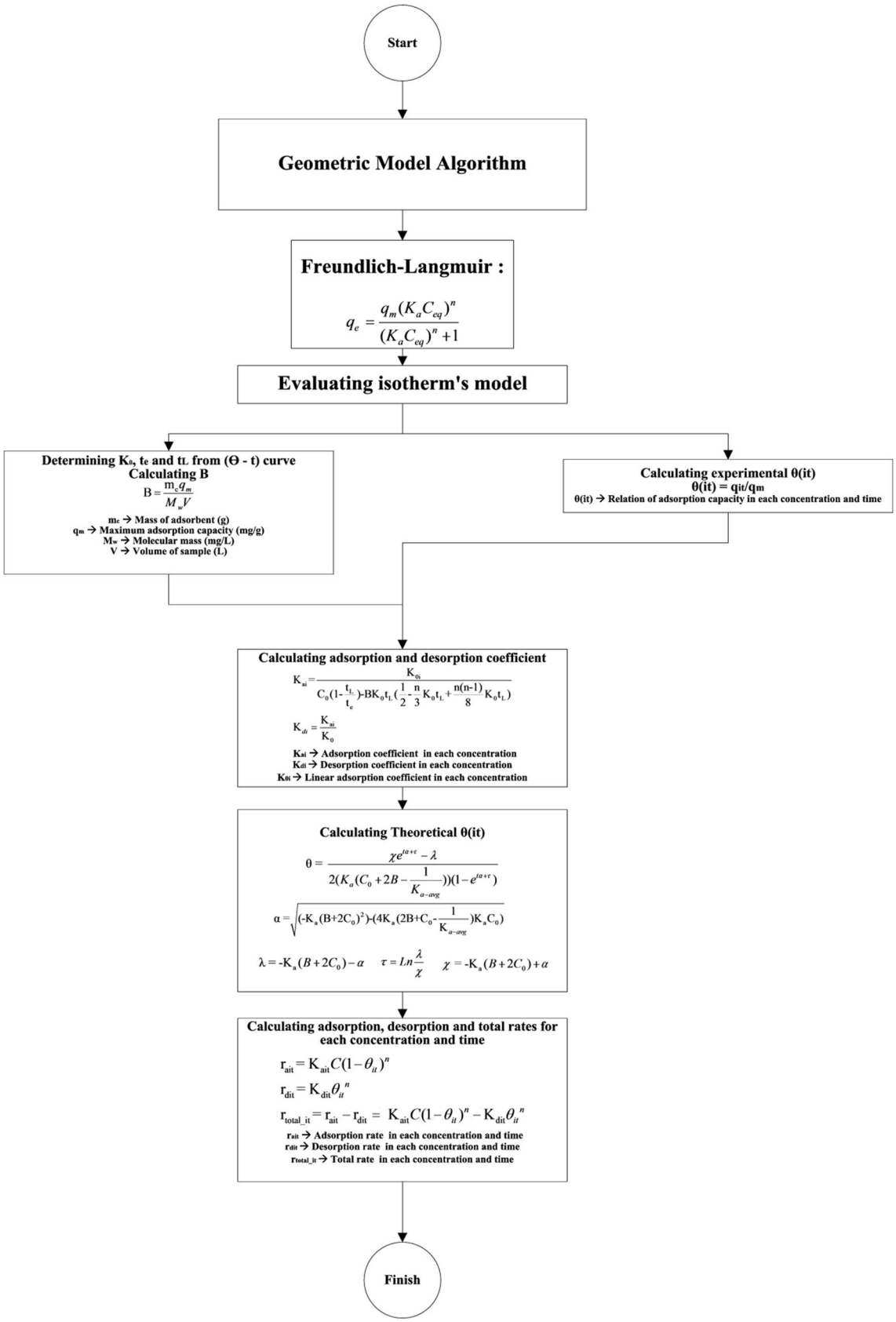

Fig. 6 Geometric model calculation equation algorithm

diffusion is affected by the adsorption process. Therefore, intraparticle diffusion and surface adsorption have main roles in the adsorptive reactions at the same time (Bulut et al., 2008).

Boyd plot

The Boyd plot is able to estimate the real slowest step in the adsorption reaction. This Kinetic mathematical equation is expressed in Eq. 22 (Vadivelan & Kumar, 2005):

$$F = 1 - (1.01364\pi)\exp B_t \tag{22}$$

$$F = \frac{q_t}{q_e} \tag{23}$$

F known as the fractional analyte at a desired time, B_t represents a numerical concept of F, and q_t is the capacity of adsorption process at any time t (mg g^{-1}). By integrating Eqs. (22) and (23), Eq. (24) is obtained.

$$B_t = -0.4977 - \ln(1 - F) \tag{24}$$

If the B_t versus t graph is a straight line and crosses the origin of the plot, the intraparticle diffusion is the controller element of the process. Otherwise, the film diffusion is dominant and considered as the reaction-controlling stage (49, 50). Subsequently, the values of the effective diffusion coefficient could get calculated by Eq. 25:

$$B = \frac{\pi^2 D_i}{r_i^2} \tag{25}$$

r_i is the mean radius of CAAC particles and Di is the effective diffusion of dyes onto the CAAC surface (Hameed, 2008). The gained values of the Boyd kinetic model constants including B and D_i are listed in Table S4 (amounts of R^2 for this model are in 0.964 and 0.994 range). It was observed from Fig. S10-S12 that the curves were linear and did not cross the origin. Therefore, the adsorption procedure was controlled by film diffusion (external diffusion) rather than intraparticle diffusion (internal diffusion) in each dye. So, the pseudo-first-order is the most accurate model for all of the adsorptive reaction; besides, the Elovich equation also provides the experimental data close to the calculated ones.

The mean radius of CAAC particles obtained from SEM images is approximately 1.2 µm, and the values of D_i were calculated as shown in Table S4. By calculating of D_i values for all dyes (Table S4 and Fig. S13), it was obtained that all concentrations of MV, MB and MG have higher D_i values, respectively, as shown in the comparative bar diagram. As the straight relationship exists between Di values and the diffusion coefficient in mass transfer process, MV has better mass transfer than other dyes.

Geometric model

The main part of geometrical model is to study the mechanism of adsorption/desorption and their change rates over time in the adsorption process (Eftekhari et al., 2021). Calculations of the geometric model are presented in an algorithm represented in Fig. 6. By inserting the required data into the equations obtained in the mentioned algorithm, the adsorption/desorption rate plots are drawn in Figs. S14-S16.

According to Figs S14-S16, it is detectable that at all concentrations for MG and MB, the adsorption process appeared perfectly due to the lack of intersection between the adsorption and desorption rate graphs. Moreover, this scenario repeats for MV dye at dosages of 50, 100 and 200 mg L^{-1}. Nonetheless, according to Fig. S16, part d, due to the steep slope of the adsorption rate curve, it can be deduced that the rate of adsorption reduction at this concentration was higher for MV, and thus the adsorbent regeneration should be performed in a shorter time. Considering θ, the kinetics model of the adsorption process can be predicted. With considering the theoretical and empirical θ values, the amounts of adsorption capacity could be predicted by high accuracy (Boyd et al., 1947; Sadeghalvad et al., 2017). For example, for both Fig. S17 and S18, parts a, b and c, which corresponds to the experimental and predicted θ of MG and MB at different dosages of 50, 100 and 200 mg L^{-1}, respectively, the kinetics of the experiment could be well predicted. However, for part d, in both Figs. S17 and S18 as well as in all parts of Fig. S19, experiment θ and the calculated θ curves have low versatility indicating that these plots are incapable of predicting the actual kinetics for MV dye at all concentrations and MB and MG at 400 mg L^{-1}.

Comparison to other adsorbent

CAAC as a low-cost adsorbent obtained from the construction waste reached Q_{max} values of 370.4, 256.4 and 277.8 mg g^{-1} for MG, MB, and MV dyes, correspondingly. The efficiency of the proposed CAAC powder is compared with other adsorbents for the treatment of MV, MG and MB, and the results are listed in Table S5. Application of CAAC as adsorbent provides sustainable development goals regarding the clean water, development of industry and infrastructure and sustainable cities and society.

Conclusion

CAAC waste has used as a refining material for wastewater treatment plant (WWTP) facilities to seize sustainable development goals (SDGs) and circular economy (CE) concept. Thus, CAAC waste was utilized as an efficient adsorbent to remove cationic dyes such as MV, MG and MB from water samples. To probe the adsorption process, five kinetic models were studied and based on the obtained results, the adsorption of MG, MB and MV onto the CAAC powder could be explained by the pseudo-first-order, Elovich equations and Boyd mathematical model for all dyes. Also, film diffusion plays more important and efficient role than intraparticle diffusion. Besides, the experimental isotherm data were explored by using two-parameter (Dubinin-Radushkevich, Temkin, Freundlich, and Langmuir equations) and three-parameter models (Toth, Sips, Redlich-Peterson and Koble-Corrigan models). Based on the results, the adsorption of MG and MB onto the CAAC powder followed the Langmuir isotherm; however, adsorption of MV obeyed the Freundlich isotherm. Moreover, geometric equations have shown generally optimized conditions for adsorption/desorption process of dyes. Consequently, as CAAC adsorbent is available from wastes of constructions and besides its low costs for preparation; these advantages make it a unique adsorbent to remove the cationic dyes.

Supplementary Information The online version contains supplementary material available at https://doi.org/10.1007/s13762-021-03576-9.

Acknowledgements The first and second authors would like to thank Mrs. Mahsa Keramati and Melorin Eftekhari for their conscientiously support to collect the data for this project. We also wish to thank the Editor-in-Chief and anonymous reviewers for their constructive and very useful suggestions.

Authors contributions MG was involved in experimental activities; formal analysis; investigation; methodology; review & editing; ME was involved in supervision; project admiration; review & editing; MGT was involved in novel computations; draft preparation; review & editing; **AMF-F** was involved in review & editing; **GT** was involved in review & editing.

Funding The authors declare that there is no finding for this research.

Availability of data and materials The authors declare that the data are available and can be presented upon the requested of the readers.

Declarations

Conflict of interest The authors declared that they have no conflict of interest.

Consent to participate The authors declare that they agree to participate based on the journal's format.

Consent to publish The authors declare that they agree with the publication of this paper in this journal.

Ethical approval The authors declare that there is no conflict of interest.

References

Al-Bastaki N (2004) Removal of methyl orange dye and Na2SO4 salt from synthetic waste water using reverse osmosis. Chem Eng Process 43(12):1561–1567

Al-Kinani A, Gheibi M, Eftekhari M (2019) Graphene oxide–tannic acid nanocomposite as an efficient adsorbent for the removal of malachite green from water samples. Modeling Earth Systems and Environment 5:1627–1633

Azizian S, Haerifar M, Basiri-Parsa J (2007) Extended geometric method: a simple approach to derive adsorption rate constants of Langmuir-Freundlich kinetics. Chemosphere 68(11):2040–2046

Bhattacharyya R, Ray SK (2015) Removal of congo red and methyl violet from water using nano clay filled composite hydrogels of poly acrylic acid and polyethylene glycol. Chem Eng J 260:269–283

Bouabidi ZB, El-Naas MH, Cortes D, McKay G (2018) Steel-Making dust as a potential adsorbent for the removal of lead (II) from an aqueous solution. Chem Eng J 334:837–844

Boyd, G. E., Adamson, A. W., & Myers Jr, L. S. (1947). The exchange adsorption of ions from aqueous solutions by organic zeolites. II. Kinetics1. *Journal of the American Chemical Society*, *69*(11), 2836–2848.

Bulut E, Özacar M, Şengil İA (2008) Adsorption of malachite green onto bentonite: equilibrium and kinetic studies and process design. Microporous Mesoporous Mater 115(3):234–246

Eftekhari, M., Gheibi, M., Azizi-Toupkanloo, H., Hossein-Abadi, Z., Khraisheh, M., Fathollahi-Fard, A.M., Tian, G. (2021). Statistical optimization, soft computing prediction, mechanistic and empirical evaluation for fundamental appraisal of copper, lead and malachite green adsorption. *Journal of Industrial Information Integration*, *23*, 100219.

Fathollahi-Fard, A. M., Ahmadi, A., & Al-e-Hashem, S. M. (2020a). Sustainable closed-loop supply chain network for an integrated water supply and wastewater collection system under uncertainty. *Journal of Environmental Management*, *275*, 111277.

Fathollahi-Fard AM, Hajiaghaei-Keshteli M, Tian G, Li Z (2020b) An adaptive Lagrangian relaxation-based algorithm for a coordinated water supply and wastewater collection network design problem. Inf Sci 512:1335–1359

Fathollahi-Fard, A. M., Woodward, L., & Akhrif, O. (2021). Sustainable distributed permutation flow-shop scheduling model based on a triple bottom line concept. *Journal of Industrial Information Integration*, 100233.

Fu J, Chen Z, Wang M, Liu S, Zhang J, Zhang J, Han R, Xu Q (2015) Adsorption of methylene blue by a high-efficiency adsorbent (polydopamine microspheres): kinetics, isotherm, thermodynamics and mechanism analysis. Chemical Engineering Journal 259:53–61

Gillman PK (2011) CNS toxicity involving methylene blue: the exemplar for understanding and predicting drug interactions that precipitate serotonin toxicity. J Psychopharmacol 25(3):429–436
Hamad AJ (2014) Materials, production, properties and application of aerated lightweight concrete. International Journal of Materials Science and Engineering 2(2):152–157
Hameed BH, El-Khaiary MI (2008) Malachite green adsorption by rattan sawdust: Isotherm, kinetic and mechanism modeling. J Hazard Mater 159(2–3):574–579
Hameed B (2008) Equilibrium and kinetic studies of methyl violet sorption by agricultural waste. J Hazard Mater 154(1–3):204–212
Hartmann A, Buhl JC (2012) Reaction Behavior of Autoclaved Aerated Concrete and Sodium Aluminate at Mild Alkaline and Acid Hydrothermal Conditions: Model for AAC Recycling. J Mater Civ Eng 24(4):441–450
Hashimoto JC, Paschoal JAR, De Queiroz JF, Reyes FGR (2011) Considerations on the use of malachite green in aquaculture and analytical aspects of determining the residues in fish: a review. J Aquat Food Prod Technol 20(3):273–294
Hor KY, Chee JMC, Chong MN, Jin B, Saint C, Poh PE, Aryal R (2016) Evaluation of physicochemical methods in enhancing the adsorption performance of natural zeolite as low-cost adsorbent of methylene blue dye from wastewater. J Clean Prod 118:197–209
Jerman M, Keppert M, Výborný J, Černý R (2013) Hygric, thermal and durability properties of autoclaved aerated concrete. Constr Build Mater 41:352–359
Jossens L, Prausnitz JM, Fritz W, Schlünder EU, Myers AL (1978) Thermodynamics of multi-solute adsorption from dilute aqueous solutions. Chem Eng Sci 33(8):1097–1106
Khan TA, Khan EA (2015) Removal of basic dyes from aqueous solution by adsorption onto binary iron-manganese oxide coated kaolinite: non-linear isotherm and kinetics modeling. Appl Clay Sci 107:70–77
Koble RA, Corrigan TE (1952) Adsorption isotherms for pure hydrocarbons. Ind Eng Chem 44(2):383–387
Kumar KV (2006) Comparative analysis of linear and non-linear method of estimating the sorption isotherm parameters for malachite green onto activated carbon. J Hazard Mater 136(2):197–202
Kumar A, Jena HM (2016) Removal of methylene blue and phenol onto prepared activated carbon from Fox nutshell by chemical activation in batch and fixed-bed column. J Clean Prod 137:1246–1259
Kuppusamy S, Thavamani P, Megharaj M, Venkateswarlu K, Lee YB, Naidu R (2016) Potential of Melaleuca diosmifolia as a novel, non-conventional and low-cost coagulating adsorbent for removing both cationic and anionic dyes. J Ind Eng Chem 37:198–207
Kushwaha AK, Gupta N, Chattopadhyaya MC (2014) Removal of cationic methylene blue and malachite green dyes from aqueous solution by waste materials of Daucus carota. J Saudi Chem Soc 18(3):200–207
Liu X, Tian G, Fathollahi-Fard AM, Mojtahedi M (2020) Evaluation of ship's green degree using a novel hybrid approach combining group fuzzy entropy and cloud technique for the order of preference by similarity to the ideal solution theory. Clean Technol Environ Policy 22(2):493–512
McDougall, F.R., White, P.R., Franke, M., Hindle, P., Integrated solid waste management: a life cycle inventory. John Wiley & Sons (2008).
Mo JH, Lee YH, Kim J, Jeong JY, Jegal J (2008) Treatment of dye aqueous solutions using nanofiltration polyamide composite membranes for the dye wastewater reuse. Dyes Pigm 76(2):429–434
Moghaddam SS, Moghaddam MA, Arami M (2010) Coagulation/flocculation process for dye removal using sludge from water treatment plant: optimization through response surface methodology. J Hazard Mater 175(1–3):651–657
Mohan D, Singh KP (2002) Single-and multi-component adsorption of cadmium and zinc using activated carbon derived from bagasse—an agricultural waste. Water Res 36(9):2304–2318
Mojtahedi, M., Fathollahi-Fard, A. M., Tavakkoli-Moghaddam, R., & Newton, S. (2021). Sustainable Vehicle Routing Problem for Coordinated Solid Waste Management. *Journal of Industrial Information Integration*, 100220.
Nataraj SK, Hosamani KM, Aminabhavi TM (2009) Nanofiltration and reverse osmosis thin film composite membrane module for the removal of dye and salts from the simulated mixtures. Desalination 249(1):12–17
Nekouei F, Nekouei S, Tyagi I, Gupta VK (2015) Kinetic, thermodynamic and isotherm studies for acid blue 129 removal from liquids using copper oxide nanoparticle-modified activated carbon as a novel adsorbent. J Mol Liq 201:124–133
Pérez-Marín AB, Zapata VM, Ortuno JF, Aguilar M, Sáez J, Lloréns M (2007) Removal of cadmium from aqueous solutions by adsorption onto orange waste. J Hazard Mater 139(1):122–131
Porkodi K, Kumar KV (2007) Equilibrium, kinetics and mechanism modeling and simulation of basic and acid dyes sorption onto jute fiber carbon: Eosin yellow, malachite green and crystal violet single component systems. J Hazard Mater 143(1–2):311–327
Redlich OJDL, Peterson DL (1959) A useful adsorption isotherm. J Phys Chem 63(6):1024–1024
Reife, A., Freeman, H.S. editors. Environmental chemistry of dyes and pigments. John Wiley & Sons (1996).
Robati D, Mirza B, Rajabi M, Moradi O, Tyagi I, Agarwal S, Gupta VK (2016) Removal of hazardous dyes-BR 12 and methyl orange using graphene oxide as an adsorbent from aqueous phase. Chem Eng J 284:687–697
Sabnis R.W., Handbook of biological dyes and stains: synthesis and industrial applications. John Wiley & Sons (2010).
Sadeghalvad B, Azadmehr A, Hezarkhani A (2017) Sulfate decontamination from groundwater by metal layered double hydroxides functionalized high phosphorus iron ore waste as a new green adsorbent: Experimental and modeling. Ecol Eng 106:219–230
Santhi T, Manonmani S, Smitha T (2010) Removal of malachite green from aqueous solution by activated carbon prepared from the epicarp of Ricinus communis by adsorption. J Hazard Mater 179(1–3):178–186
Saratale RG, Saratale GD, Chang JS, Govindwar SP (2011) Bacterial decolorization and degradation of azo dyes: a review. J Taiwan Inst Chem Eng 42(1):138–157
Sasmal, D., Banerjee, S., Senapati, S., & Tripathy, T. (2020). Effective removal of Th^{4+}, Pb^{2+}, Cd^{2+}, malachite green, methyl violet and methylene blue from their aqueous solution by amylopectin dialdehyde-Schiff base. *Journal of Environmental Chemical Engineering*, *8*(3), 103741.
Sips R (1948) On the structure of a catalyst surface. J Chem Phys 16(5):490–495
Srivastava S, Sinha R, Roy D (2004) Toxicological effects of malachite green. Aquat Toxicol 66(3):319–329
Suteu, D., Bilba, D., & Coseri, S. (2014). Macroporous polymeric ion exchangers as adsorbents for the removal of cationic dye basic blue 9 from aqueous solutions. *Journal of Applied Polymer Science*, *131*(1).
Tang, S. H., & Zaini, M. A. A. (2020). Development of activated carbon pellets using a facile low-cost binder for effective malachite green dye removal. *Journal of Cleaner Production*, *253*, 119970.
Tang, Y., Zhao, Y., Lin, T., Li, Y., Zhou, R., & Peng, Y. (2019). Adsorption performance and mechanism of methylene blue by H3PO4-modified corn stalks. *Journal of Environmental Chemical Engineering*, *7*(6), 103398.

Tian G, Liu X, Zhang M, Yang Y, Zhang H, Lin Y, Ma F, Wang X, Qu T, Li Z (2019) Selection of take-back pattern of vehicle reverse logistics in China via Grey-DEMATEL and Fuzzy-VIKOR combined method. Journal of cleaner production 220:1088–1100

Vadivelan V, Kumar KV (2005) Equilibrium, kinetics, mechanism, and process design for the sorption of methylene blue onto rice husk. J Colloid Interface Sci 286(1):90–100

Vankar PS (2000) Chemistry of natural dyes. Resonance 5(10):73–80

Verma Y (2008) Acute toxicity assessment of textile dyes and textile and dye industrial effluents using Daphnia magna bioassay. Toxicol Ind Health 24(7):491–500

Vijayaraghavan K, Padmesh TVN, Palanivelu K, Velan M (2006) Biosorption of nickel (II) ions onto Sargassum wightii: application of two-parameter and three-parameter isotherm models. J Hazard Mater 133(1–3):304–308

Wang, W., Tian, G., Chen, M., Tao, F., Zhang, C., Abdulraham, A. A., ... & Jiang, Z. (2020). Dual-objective program and improved artificial bee colony for the optimization of energy-conscious milling parameters subject to multiple constraints. *Journal of Cleaner Production*, *245*, 118714.

Weng CH, Pan YF (2007) Adsorption of a cationic dye (methylene blue) onto spent activated clay. J Hazard Mater 144(1–2):355–362

Yang Q, Zhong Y, Li X, Li X, Luo K, Wu X, Chen H, Liu Y, Zeng G (2015) Adsorption-coupled reduction of bromate by Fe (II)–Al (III) layered double hydroxide in fixed-bed column: experimental and breakthrough curves analysis. J Ind Eng Chem 28:54–59

Yang Y, Yuan G, Zhuang Q, Tian G (2019) Multi-objective low-carbon disassembly line balancing for agricultural machinery using MDFOA and fuzzy AHP. J Clean Prod 233:1465–1474

Yu P, Kirkpatrick RJ, Poe B, McMillan PF, Cong X (1999) Structure of calcium silicate hydrate (C-S-H): Near-, Mid-, and Far-infrared spectroscopy. J Am Ceram Soc 82(3):742–748

Yu, H., Dai, H, Tian, G., Wu, B., Xie, Y., Zhu, Y., Zhang, T., Fathollahi-Fard, A. M., He, Q., & Tang, H. (2021). Key technology and application analysis of quick coding for recovery of retired energy vehicle battery, *Renewable and Sustainable Energy Reviews*, *135*, 110129.

Yuan, G., Yang, Y., Tian, G., & Zhuang, Q. (2020). Comprehensive evaluation of disassembly performance based on the ultimate cross-efficiency and extension-gray correlation degree. *Journal of Cleaner Production*, *245*, 118800.

Zaitan H, Binachi D, Achak O, Chafik T (2008) A comparative study of the adsorption and desorption of o-xylene onto bentonite clay and alumina. J Hazard Mater 153:852–859